Chapter 8
Experimental Bench for the Analysis of Belt Deformation in Belt–Pulley Systems by Digital Image Correlation

Francesco Bucchi, Francesco Frendo, and Paolo Neri

Abstract Belt–pulley transmissions are a classical topic in mechanical engineering, usually studied following two approaches: the *creep* theory (Euler or Grashof model) and the *shear* theory. Recently, the authors introduced a new theory to study the belt–pulley contact mechanics, which is inspired to the *brush* model used for pneumatic tires. Basing on this theory, the belt is considered as an almost axially rigid tension member connected to a series of bristles, which are, at the other end, in contact with the pulley. In this paper, a test bench is presented and designed to experimentally validate the brush model. The bench is made up of two pulleys connected to two shafts driven by independently controlled motors; a belt is installed between the pulleys, and the shafts are equipped with sensors measuring the angular velocity and the transmitted torque. The belt preload, which is measured by a load cell, can be varied by changing the distance between the two shafts. The belt was painted creating a suitable texture (random speckle pattern) to be interpreted using the Digital Image Correlation (DIC) technique. The first results obtained by carrying out tests at low speed with different transmitted torque values are discussed, appreciating the variation in the tension of the belt along the winding arc and the dependence of the radial compression of the belt from the transmitted torque. The tangential deformation of the belt under the action of different torque values and direction of rotation of the pulleys is also presented, which is consistent with that foreseen by the brush model.

Keywords Belt · Power transmissions · Brush model · Experimental bench · Digital image correlation · Creep model

F. Bucchi (✉) · F. Frendo · P. Neri
Department of Civil and Industrial Engineering, University of Pisa, Largo L. Lazzarino, 56122 Pisa, Italy
e-mail: francesco.bucchi@unipi.it

L. F. M. da Silva (ed.), *Materials Design and Applications IV*,
Advanced Structured Materials 168, https://doi.org/10.1007/978-3-031-18130-6_8

8.1 Introduction

Pulley–belt is a transmission system used in many industrial applications, due to its low cost, ease of implementation and maintenance requirements. Several models have been proposed to study the contact mechanics, transmission capability and the overall transmission efficiency. Euler proposed the first analyses on this topic in the XVIII century, with reference to the friction of a rope wound along a pulley. In the XIX century, Reynolds and Grashof added to the Euler analyzes the effect of speed losses due to belt deformation and the centrifugal effect. More recently, the Grashof model, mentioned in the literature as creep model, was extended. According to the creep model, the winding arc is subdivided into an adhesion arc, located at the beginning of the contact arc, and a sliding arc, located nearby the exit from the pulley. Basing on this model, along the former arc, no tangential stress occurs between the belt and the pulley and, consequently, the belt tension does not vary. Along the sliding arc, the model assumes that micro-slip (creep) occurs which originates tangential friction between the belt and the pulley and, in turn, the tension variation in the belt.

In 1970, Firbank proposed an alternative model, called shear model, which assumes that friction occurs along the whole winding arc, which is divided into a region where static friction occurs, and the belt is subject to angular deformation (shear), followed by a creep region where sliding occurs. The tangential friction along both regions contributes to the torque transmission and the belt tension varies along the whole winding arc. The Firbank model has also been extended to include extensible belts (Kong and Parker 2005).

Recently, the authors proposed an innovative model (Frendo and Bucchi 2020a), which is inspired to the brush model which is usually employed for pneumatic tires of vehicles (Bernard et al. 1977; Pacejka and Sharp 1991). This model can describe the tangential stress distribution between the pulley and the belt in steady-state conditions and to predict the angular velocity of the driven pulley when a known torque value is applied to it. This allows also to estimate the power losses of the transmission system and the elastic deformation of the belt (Bertini et al. 2014; Frendo and Bucchi 2020b). Even in this model, the winding arc is divided into different regions, depending on the friction condition, and several studies have been proposed varying the transmission parameters (Bucchi and Frendo 1038). The model was also validated by finite element analyses (Bucchi and Frendo 2022) which demonstrated the capability of this approach to reproduce, through analytical expressions, the pressure and tangential force along the winding arc, except for the pulley entrance and exit zone, were kinematic issues arise (Wasfy et al. 2016); the FE analyses also showed that the hypothesis of no tension variation along the adhesion zone, postulated by Grashof, is not strictly correct.

To the best of the authors knowledge, few studies (Della and Timpone 2013) have been devoted to the experimental study of the contact mechanics between the pulley and the belt and none of them used full-field measurements.

To fill this gap, in this paper, a test bench is presented, designed to experimentally validate the brush model developed by the authors. The bench is made up of two

pulleys connected to two shafts driven by independently controlled motors; a flat belt is installed between the pulleys, and the shafts are equipped with sensors. The belt was painted creating a suitable texture (random speckle pattern) to be interpreted using the Digital Image Correlation (DIC) technique (Barone et al. 2017; Neri et al. 2022) to measure the belt deformation and, consequently, assess the pressure and tangential actions between the belt and the pulley.

Section 8.2 recaps the key features of the brush model applied to pulley–belt transmissions. Section 8.3 details the test bench layout, describing its functioning principle and its measure capabilities. Section 8.4 recaps the DIC technique fundamentals and describes the analyses performed on the acquired images. Section 8.5 shows and discusses the results in terms of belt–pulley pressure, tangential actions, belt tension and their affinity with literature models. Conclusions are drawn in Sect. 8.6.

8.2 Brush Model Outline

The first basic hypothesis of the "brush model" is considering the belt as made of two parts: the rubber matrix being in contact with the pulley along the winding arc, and the reinforcement fibers, having the stiffness several orders of magnitude greater than the rubber matrix stiffness. The belt is assumed as a planar component, and no stress component arise along the belt width (transverse direction). In the first version of the brush model (Frendo and Bucchi 2020a), which is used in this work, the reinforcement fibers are inextensible. The same model can also be applied to belts having elastic reinforcement fibers.

The model assumes that a bed of elastically deformable bristles composes the rubber matrix. Such bristles are connected to the tension member on one end and are in contact with the pulley on the other end.

The bristles height is negligible with respect to the pulley radius, and they are ideally elastic, deformable along the tangential direction due to the speed difference between the belt inextensible tension member, which has constant speed V_b in steady-state condition, and the pulley.

If the bristle tangential deformation s is known, the contact tangential stress τ given by Eq. 8.1:

$$\tau = k_s s \tag{8.1}$$

where the parameter k_s is the bristle tangential stiffness. In order to determine the bristle tangential deformation s, two different cases are discussed, depending on the fact that the analyzed pulley is driving or driven.

Considering the belt entering in the driving the pulley, having radius R_{dg} and angular speed ω_{dg}, the bristle deformation along the driving pulley s_{dg} is expressed as a function of the angular coordinate α as follows

$$s_{\mathrm{dg}}(\alpha) = \int_0^{\alpha} \frac{V_{\mathrm{s,\,dg}}}{\omega_{\mathrm{dg}}} \mathrm{d}\tilde{\alpha} = \frac{V_{\mathrm{s,\,dg}}}{\omega_{\mathrm{dg}}} \alpha \tag{8.2}$$

where $V_{\mathrm{s,\,dg}} = \omega_{\mathrm{dg}} R_{\mathrm{dg}} - V_{\mathrm{b}}$ is the relative slip velocity of the belt. Equation 8.2 is valid if the static friction between the belt and the pulley is enough to bear the tangential stress, that is

$$\tau_{\mathrm{dg}}(\alpha) = k_{\mathrm{s}} \frac{V_{\mathrm{s,\,dg}}}{\omega_{\mathrm{dg}}} \alpha \leq f_{\mathrm{s}} p_{\mathrm{dg}} \tag{8.3}$$

where f_{s} is the static friction coefficient and p_{dg} is the normal pressure between the belt and the pulley. The normal pressure is computed considering the radial equilibrium of the belt and is expressed by

$$p_{\mathrm{dg}}(\alpha) = \frac{T_{\mathrm{dg}}(\alpha) - q V_{\mathrm{b}}^2}{R_{\mathrm{dg}}} \tag{8.4}$$

being $T_{\mathrm{dg}}(\alpha)$ the belt tension along the driving pulley and q the lineic mass. The belt tension is obtainable integrating the tangential stress along the winding arc of the driving pulley. The static friction limit is then reached for a precise value of α (Frendo and Bucchi 2020a). Then, the friction regime moves from static to kinematic, usually reducing the friction coefficient. This effect produces stick-slip phenomenon along the slip zone, described in detail in Frendo and Bucchi 2020a. The tangential stress along the winding arc reduces along the sliding arc, as well as the normal pressure and the belt tension. Figure 8.1a shows an exemplificative trend of the tangential stress along the winding arc. The friction static [kinematic] limit is also shown, which is computed multiplying the normal pressure and the static [kinematic] friction coefficient. Hence, Fig. 8.1a provides also information related to the normal pressure trend. Figure 8.1b shows the belt tension along the winding arc of the driving pulley.

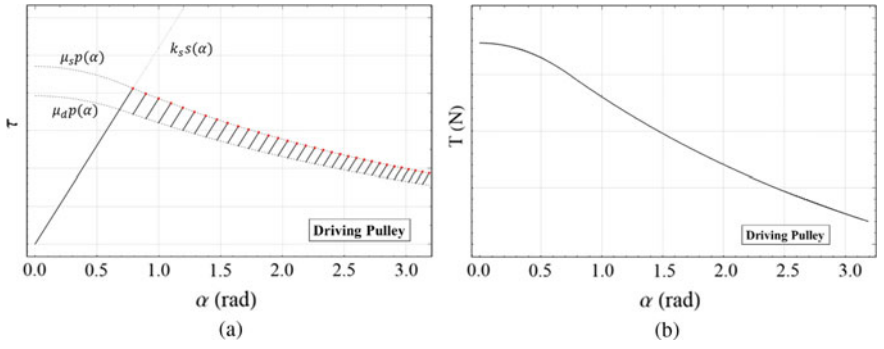

Fig. 8.1 Tangential stress (**a**) and belt tension (**b**) along the winding arc of the driving pulley (Frendo and Bucchi 2020a)

It is worth noting that the tangential stress linearly rises with α up to its maximum value, which occurs where the static friction limit is reached and then decreases. The normal pressure and the belt tension, which are directly proportional if the centrifugal effect is neglected (e.g. at low speed, see Eq. 8.4), decreases along the whole winding arc.

Concerning the driven pulley, a similar approach can be used, precisely described in Frendo and Bucchi 2020a. In such a case, the tangential stress, as well as the pressure and the belt tension, increases (if the local stick-slip phenomenon is neglected) along the winding arc.

8.3 Test Bench Description

In order to experimentally validate the brush model, a dedicated test bench was conceived. The aim of the bench was to control the angular velocity of the driving pulley and the resistant moment at the driven pulley of a dummy transmission system composed of a flat belt and two pulleys. A belt with reinforcement fibers was chosen to be used as flat belt. Due to difficulties in finding commercial flat reinforced belts, a commercial trapezoidal belt was selected, but it was used as flat belt, using the internal surface of the belt in contact with the external cylindrical surface of the pulley.

Figure 8.2 shows a picture of the test bench installed in the University of Pisa laboratory, and Fig. 8.3 shows a schematic of the data acquisition system and control logic of the test bench.

A brushless motor (BM), driven by the brushless driver (BD, not represented in Fig. 8.2), controllable either through an integrated speed control (SC) or torque control (TC), is connected to the left shaft, which is supported by two bearings. The shaft is equipped with a torque (torsiometer) and angular position/velocity (encoder) sensor, measuring the left shaft torque T_L and angular velocity ω_L, respectively. At the end of the shaft, the pulley is fixed. The whole left shaft system (motor, shaft, pulley and sensor) is installed on a sleeve whose position can be regulated by a screw. This allows to set the desired belt pre-tension.

On the other side, an asynchronous motor (AM), driven by the asynchronous drive (AD, not represented in Fig. 8.2), is connected to the right shaft, which is also equipped with a torque and angular position/speed sensor, measuring the left shaft torque T_R and angular velocity ω_R, respectively. The bearings which support the right shaft are installed on two tri-axial load cells which allow to measure the bearing forces (F_1 and F_2) and considering the shaft equilibrium, which allow to compute the belt total tension (sum of tight and loose sides of the belt, neglecting the centrifugal effect). The asynchronous motor has no integrated speed or torque control, but its speed or torque can be controlled by a PID which uses the signals measured by torque and speed sensor (Fig. 8.3 shows only the speed control case). All the measurement signals are acquired by a USB-6351 National Instrument board (DAQ), which also controls the input signal of the controllers of the motors. A

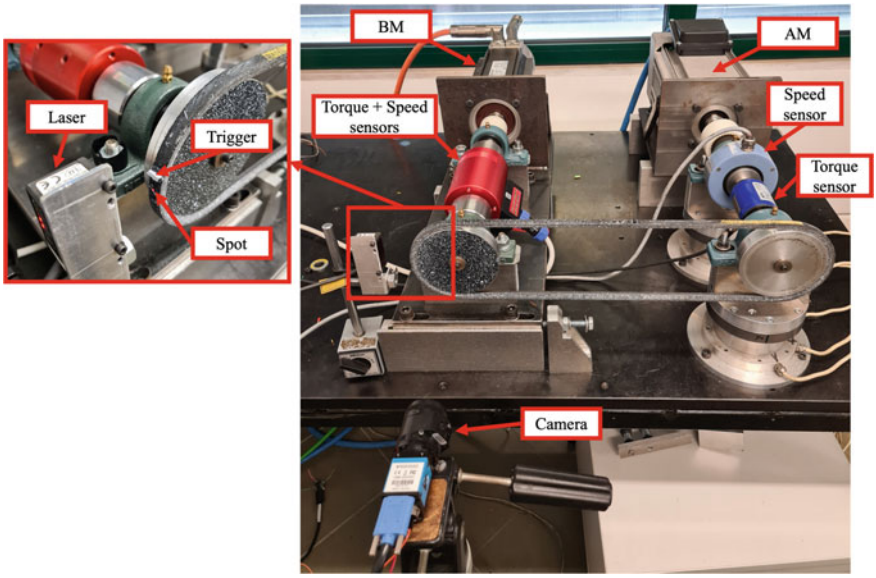

Fig. 8.2 Belt–pulley contact mechanics test bench

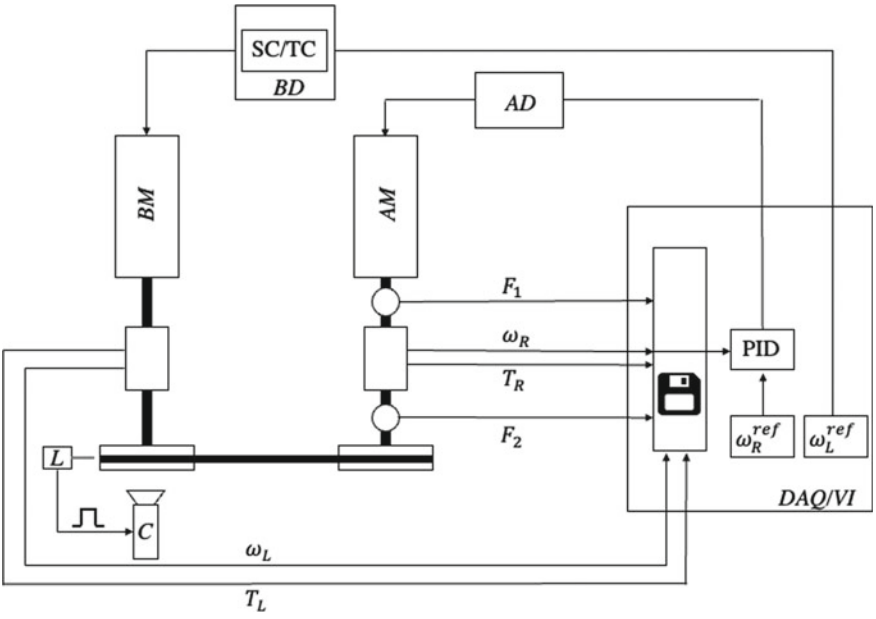

Fig. 8.3 Schematic of the logic and control of the test bench

LabVIEW virtual instrument (VI) was developed to record the data and control the motor speed.

The belt tension and pressure cannot be directly measured and, to assess them, an indirect measurement system was conceived. The image acquisition system, shown in the zoomed detail in Fig. 8.2, is made up of a camera (C) (Image sourcing DMK 23UP031), a trigger element fixed on the belt and a laser sensor (L) which detects the passage of the trigger element. Indeed, since slip occurs between the pulley and the belt, it is not possible to use the encoder installed on the pulley shaft to assess the belt position. Nevertheless, the belt has to be shot in the same position in order to correctly elaborate images using the DIC technique. For this reason, a laser sensor and a camera, which allows the trigger input, were directly connected to acquire a picture every time the trigger sensor is detected by the laser. Both the lateral surface of the belt and the frontal surface of the left pulley were painted creating a suitable texture (random speckle pattern, see Fig. 8.5), which is processed through DIC technique.

The measurement system allows to compute the belt deformation by a Digital Image Correlation (DIC) system, whose working principle is described in Sect. 8.4.

8.4 DIC Analyses Implementation

Digital Image Correlation is a well-established technique which allows for the measurement of displacements through image processing. Provided that a random pattern is available on the target object, it is possible to track the surface displacement in each frame. This can be achieved by exploiting the natural texture of the surface or, more frequently, by spraying or gluing a black and white speckle pattern on the object. Once the grid of measurement points is defined on the images, a pixel subset is associated with each point and tracked along the frame set to estimate horizontal (Δx) and vertical (Δy) displacements. This procedure is illustrated in Fig. 8.4, for two consecutive frames.

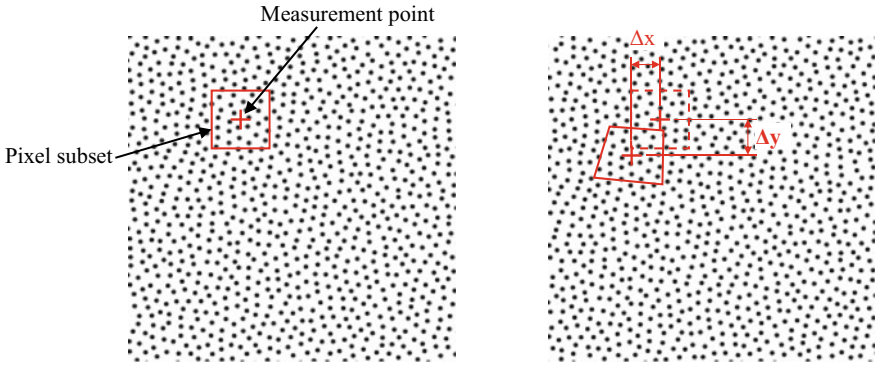

Fig. 8.4 Working principle for DIC analysis

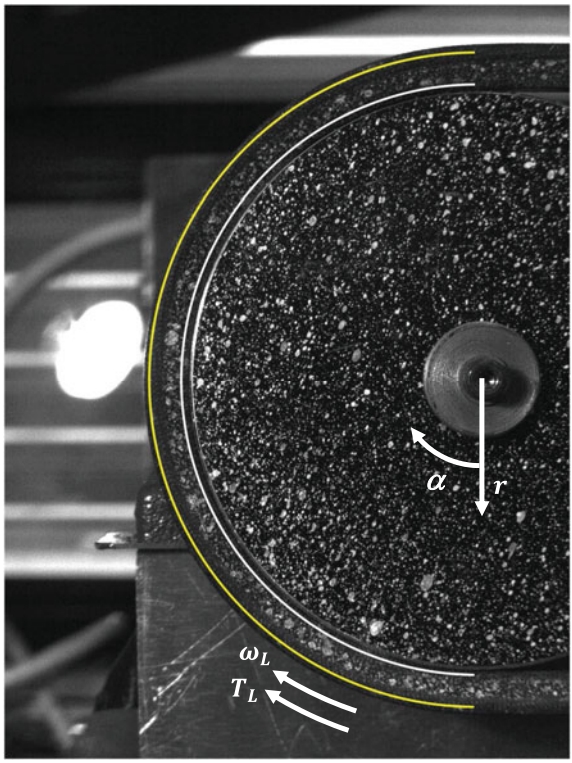

Fig. 8.5 Speckle pattern, reference system and measuring arcs on the driving pulley

In this paper, an open source 2D DIC algorithm was used to perform the task (Eberl 2010). Since the belt shows a black surface, white spray paint was used to obtain the speckle pattern, as shown in Fig. 8.5. The aforementioned algorithm provides the raw data calculation, i.e. extracting the full-field displacement information from the image set. It is worth noting that due to slip, the belt revolution period is not an integer multiple of the pulley rotation period. For this reason, the region of interest in this research is limited to the belt surface, thus, even if the speckle pattern was painted on both the pulley and the belt, only the belt measure is worth of interest. For this reason, the measurement grid was defined only on the belt area, where correlation is expected to be successful. The DIC measurement requires the definition of a reference image, which set the zero for the displacement. In this paper, the zero was set by taking a frame of the rotating belt with no torque applied to the pulley. Then, the frames were shot by subsequently increasing the torque value, thus imposing higher load to the belt, always waiting for steady-state condition. Thanks to the trigger implementation, described in Sect. 8.3, it was possible to shoot the belt at the same position, allowing to compare the images acquired for different torque values.

Three frames were taken at each torque value, to assess the measurement repeatability. The raw displacement maps are defined in the camera reference frame along the vertical and horizontal directions. Due to the typical belt deformed shape, a cylindrical reference frame centered on the pulley (Fig. 8.5) is more convenient for result interpretation. Thus, the center of the pulley was detected in the first image, by manually selecting ten points on the pulley circumference and then computing the best fitting ellipse (to account for any small misalignment between the camera and the pulley). The Cartesian raw displacement could then be converted into radial and tangential displacements. The tangential displacements were additionally normalized with respect to the distance between each measurement point and the pulley center (i.e. radius), to obtain angular displacement in radians and to allow to compare the results with the brush model, which assumes negligible belt thickness. Even if the full-field maps provide a clear and complete overview of the displacement distribution all over the belt, additional processing was performed to obtain an in-depth analysis of the results. In particular, the results corresponding to the maximum and minimum radius of the belt were selected (i.e. yellow and white line in Fig. 8.5, respectively), and the difference between radial and tangential displacements at the two radii were plotted. These results are directly related, by the knowledge of the belt radial and tangential stiffness, to the radial (pressure) and tangential stress acting between the pulley and the belt.

8.5 Test Results and Discussion

Preliminary tests were performed to assess the test bench equipment functionality. A very low speed (about 10 rpm) was imposed at the brushless motor and different constant values of resistant torque were applied using the PID implemented to control the asynchronous motor. In particular, three torque levels were imposed: (i) no resistant torque, (ii) 1.5 Nm resistant torque and (iii) 3.5 Nm resistant torque. In all the tests, in addition to the resistant torque applied by the asynchronous motor, a bias torque of 0.5 Nm had to be overcome due to bench losses (bearings).

The displacement of each point of the belt wound on the driven (brushless motor side) pulley was analyzed using DIC technique. In particular, the displacement d_r and d_t of each point of the grid were measured along the radial and tangential direction, respectively. Zero displacement refers to the torque level (i) (no resistant torque applied by the motor, only friction torque has to be overcome). Concerning the tangential displacement, to compare the displacement of different grid points having different radial coordinate, the tangential angular displacement was measured as follows:

$$d_\alpha(\alpha,\, r) = \frac{d_t(\alpha,\, r)}{r} \tag{8.5}$$

In addition, in order to analyze the tangential deformation of the belt, which is related to the tangential stress between the belt and the pulley, two arcs shown in Fig. 8.5 were selected on the grid, with the white arc corresponding to the minimum measurable radius (R_i) and the yellow arc corresponding to the maximum measurable radius (R_e) along the belt. Hence, the belt tangential deformation was defined as

$$\Delta_\alpha(\alpha) = d_\alpha(\alpha,\ R_i) - d_\alpha(\alpha,\ R_e) \tag{8.6}$$

Figure 8.6 shows the radial displacement of the belt wound on the driven pulley obtained when the resistant torque is 3.5 Nm. Since the torque applied by the brushless motor is clockwise, the tight side of the belt is on the lower part and the slack side on the upper part of the figure.

This is also confirmed analyzing the radial displacement which is negative on the bottom part of the figure and gradually changes to positive clockwise moving. The radial displacement of the belt is related to the pressure acting between the belt and the pulley and consequently, as stated in Eq. 8.4, to the belt tension (in this case, the centrifugal effect is negligible due to the very low velocity). Hence, the DIC

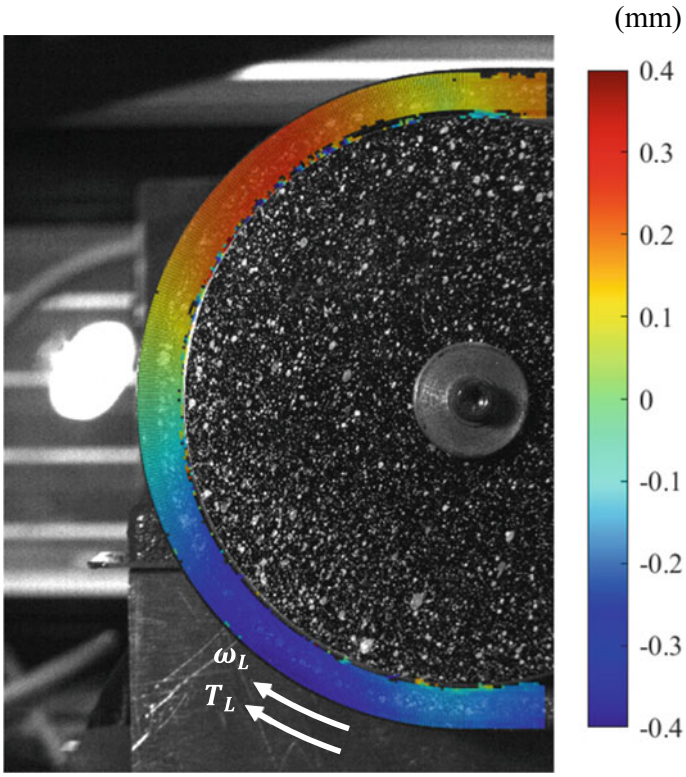

Fig. 8.6 Radial displacement of the grid elements belonging to the belt

analysis allows to measure how the belt is compressed in the lower part (entrance) and is enlarged in the lower part (exit) of Fig. 8.6, proving that the pressure and consequently the tension of the belt is higher at the pulley entrance (tight side of the belt) and lower at the pulley exit (loose side of the belt). The trend is not monotonic due to local effects at the entrance and the exit of the pulley, which will be considered in the future analysis.

Figure 8.7 shows the tangential displacement d_α for each point of the grid, for the same load condition. Neglecting the local effects nearby the entrance and exit from the pulley, all the points are subject to tangential displacement with reference to the zero-torque reference configuration; this can be attributed to small errors in the trigger setup and to the belt reinforcement fibers elasticity. It can be observed that in the central part of the winding arc, a gradient is appreciable between the angular tangential displacement at the inner and the outer radius, proving how the belt is subject to tangential stress.

To highlight the tangential deformation of the belt $\Delta_\alpha(\alpha)$ is plot in Fig. 8.8 along the whole winding arc for two different values of transmitted torque. As anticipated, $\Delta_\alpha(\alpha)$ is related (almost proportionally) to the tangential stress $\tau(\alpha)$ between the pulley and the belt. It is worth noting that the belt tangential deformation is higher as

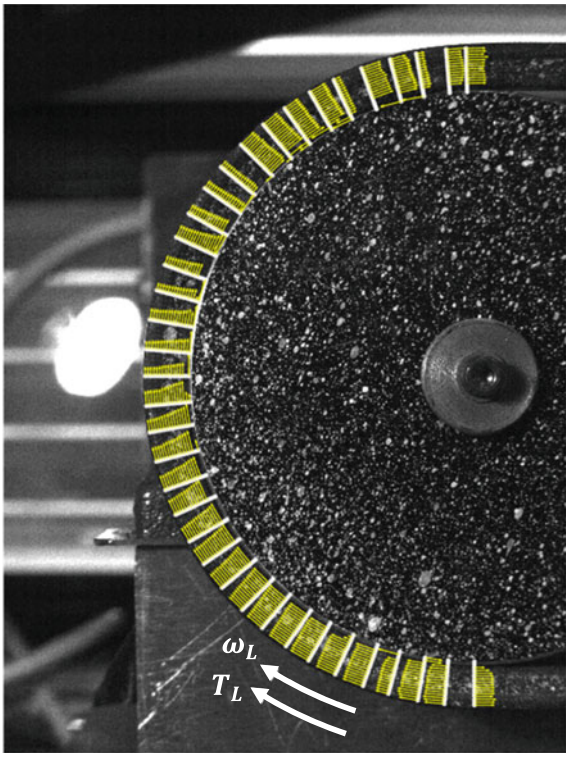

Fig. 8.7 Tangential displacement of the grid elements belonging to the belt

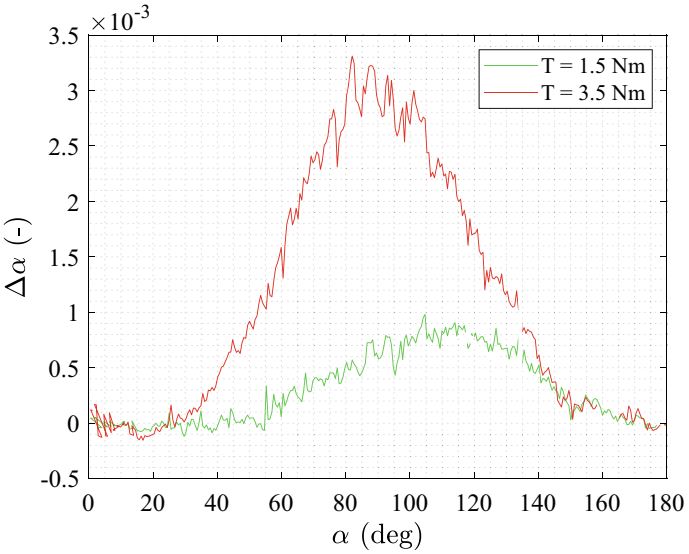

Fig. 8.8 Belt tangential deformation along the driving pulley obtained for two torque values

the transmitted torque rises, since also that the tangential stress between the pulley and the belt rises.

More worth of interest is the trend of the tangential deformation along the winding arc: neglecting the local effects at the entrance and the exit from the pulley, for both torque values $\Delta_\alpha(\alpha)$, rises almost linearly up to a maximum value. The rising slope is higher as the transmitted torque rises. Then, once the maximum value is reached, the tangential deformation decreases. This behavior is qualitatively compatible with the tangential stress plot obtained using the brush model and shown in Fig. 8.1a. Indeed, basing on the brush model, (i) $\tau(\alpha)$ linearly rises along the adhesion arc; (ii) the slope of $\tau(\alpha)$ is larger as the transmitted torque increases; (iii) $\tau(\alpha)$ reaches its maximum value when the static friction limit is reached and then decreases; (iv) the maximum value of $\tau(\alpha)$ is reached for lower values of α as the transmitted torque increases. On the contrary, if the Grashof model is considered, no tangential stress should appear along the adhesion zone and a sudden increase in the stress should verify once the slip zone is reached. This assumption seems to conflict with preliminary experimental evidence, thus confirming that the brush model is more reliable than the Grashof model.

8.6 Conclusions

In the present work, a test bench was developed to measure the contact actions between the belt and the pulley in flat belt transmissions. Two motors were used

to control the pulleys torque and speed, and a belt was painted creating a suitable texture (random speckle pattern) to be analyzed by DIC technique. Several sensors were installed on the bench, to measure the torque and angular velocity of the shaft, and a triggered camera was used to acquire belt pictures for different transmitted torque values.

A grid was created, corresponding to the belt, and the radial and tangential displacement of each point of the grid were measured for three different values of transmitted torque. The results seem promising, being the radial displacement of the belt related to the pulley–belt contact pressure and to the belt tension, and the tangential deformation related to the tangential stress between the pulley and the belt.

The preliminary results were compared with the tangential stress results obtained by the brush model, showing a fair good qualitative agreement.

In the future research, the test bench, which to the best of the authors' knowledge is novel and unique for performing such measures, will be used to collect data of a wide test campaign to characterize the belt deformation for different working conditions and compare it to theoretical and FE models results.

References

Barone S, Neri P, Paoli A, Razionale AV (2017) Digital image correlation based on projected pattern for high frequency vibration measurements. Procedia Manuf 11:1592–1599

Bernard JE, Segel L, Wild RE (1977) Tire shear force generation during combined steering and braking maneuvers. SAE technical paper, p 770852

Bertini L, Carmignani L, Frendo F (2014) Analytical model for the power losses in rubber v-belt continuously variable transmission (CVT). Mech Mach Theory 78:289–306

Bucchi F, Frendo F (2021) Analysis of belt transmissions capabilities using the brush model. IOP Conf Ser Mater Sci Eng 1038(1). IOP Publishing

Bucchi F, Frendo F (2022) Validation of the brush model for the analysis of flat belt transmissions in steady-state conditions by finite element simulation. Mech Mach Theory 167:104556

Della Pietra L, Timpone F (2013) Tension in a flat belt transmission: experimental investigation. Mech Mach Theory (70):129–156

Eberl C (2010) Digital image correlation and tracking. Mathworks, Matlab Central

Frendo F, Bucchi F (2020a) "Brush model" for the analysis of flat belt transmissions in steady-state conditions. Mech Mach Theory 143:103653

Frendo F, Bucchi F (2020b) Enhanced brush model for the mechanics of power transmission in flat belt drives under steady-state conditions: effect of belt elasticity. Mech Mach Theory 153:103998

Kong L, Parker RG (2005) Microslip friction in flat belt drives. Proc Inst Mech Eng C J Mech Eng Sci 10(219):1097–1106

Neri P, Paoli A, Santus C (2022) Stereo-DIC measurements of a vibrating bladed disk: in-depth analysis of full-field deformed shapes. Appl Sci 11

Pacejka HB, Sharp RS (1991) Shear force development by pneumatic tyres in steady state conditions: a review of modelling aspects. Veh Syst Dyn 3–4(20):121–175

Wasfy TM et al (2016) Effect of flat belt thickness on steady-state belt stresses and slip. J Comput Nonlinear Dyn 11(5)